2024-01-2550 Published 09 Apr 2024

Integrated Chassis Control for Energy-Efficient Operation of a 2WD Battery-Electric Vehicle with In-Wheel Propulsion

Marius Heydrich and Thomas Mitsching Technische Universität Ilmenau

Sebastian Gramstat Audi AG

Matthias Lenz and Valentin Ivanov Technische Universität Ilmenau

Citation: Heydrich, M., Mitsching, T., Gramstat, S., Lenz, M. et al., "Integrated Chassis Control for Energy-Efficient Operation of a 2WD Battery-Electric Vehicle with In-Wheel Propulsion," *SAE Int. J. Advances & Curr. Prac. in Mobility* 7(1):570-580, 2025, doi:10.4271/2024-01-2550.

This article was presented at the WCX SAE World Congress Experience, April 16-18, 2024.

Received: 25 Oct 2023 Revised: 30 Jan 2024 Accepted: 12 Jan 2024

Abstract

Battery-electric vehicles (BEVs) require new chassis components, which are realized as mechatronic systems mainly and support more and more by-wire functionality. Besides better controllability, it eases the implementation of integrated control strategies to combine different domains of vehicle dynamics. Especially powertrain layouts based on electric in-wheel machines (IWMs) require such an integrated approach to unfold their full potential.

The present study describes an integrated, longitudinal vehicle dynamics control strategy for a battery electric sport utility vehicle (SUV) with an electric rear axle based on in-wheel propulsion. Especially the influence of electronic brake force distribution (EBD) and torque blending control on the overall performance are discussed and demonstrated through experiments and driving cycles on public road and benchmarked to results of previous studies derived from [1]. It is shown that the approach improves energy efficiency and energy recovery potential by nearly ten per cent.

Introduction

Most vehicle dynamics control and safety systems are limited to one domain and one actuator solely e. g., anti-lock braking system and electronic stability control use the friction brakes for longitudinal dynamics control, while lane keeping systems use the steering system for assisting by maneuvers with distinct lateral dynamics. Hence, potentials of other available vehicle systems could not be fully used, since e. g. pitch and roll dynamics are influencing longitudinal and lateral dynamics as well. Therefore, it seems logical to achieve synergies from combined operation of different actuators for more efficient vehicle dynamics control systems. Integrated chassis control (ICC) describes the manipulation of one or more (vehicle) dynamics domains by more than one actuator at the same time. This approach can help to overcome actuator limitations and to create redundancy [2] by using different actuators to further enhance active safety, vehicle stability, agility and ride comfort [3]. Several studies and possible use cases were already exploited in other articles as well as surveys published in the past, see [4, 5].

Recently, a high number of articles discussing various ICC aspects focuses on the lateral vehicle dynamics, especially towards improved cornering capability and overall stability. This meets the expectation, since [3, 6] already proposed high potential of combined lateral and vertical dynamics control, so classic Electronic Stability Control (ESC) [6, 7, 8, 9, 10, 11, 14, 15, 18] or Direct Yaw Control (DYC) [12, 14, 16, 19] gets enhanced through other chassis actuators like Active Front (AFS) [6, 7, 8, 9, 11, 12, 13, 14, 15, 16, 17, 18, 19] and Active Rear Steering (ARS) [6, 8, 10, 19], Active Suspension (AS) [6, 11, 15, 17], Active Roll-Moment Control (ARC) [7, 10, 14, 16] or Torque Vectoring (TV) [8, 11, 13]. In many studies, the use of more than one actuator showed improved vehicle performance and cornering stability. Not worth noticing, the literature review demonstrates a high impact on integrated control approaches for improved lateral dynamics and path tracking capabilities. Anyway, these systems are focusing on handling limits, so in most everyday driving situations they are not getting activated. Moreover, many vehicles – especially in the lower price segments – do not have all necessary chassis actuators

on board. Therefore, other principles and dynamics control systems shall be considered in such cases. In particular, the domain of longitudinal dynamics is interesting: for acceleration, the powertrain and propulsion system has to get over the driving resistance, while the brake system has to dissipate kinetic energy for deceleration. These processes are highly relevant e. g., for studies on power consumption of a vehicle. That is why common consumption tests (e. g., WLTC, NEDC) are limited to longitudinal dynamics solely.

Especially in the domain of hybrid (HEVs) and battery electric vehicles (BEVs), energy consumption and overall efficiency are crucial points and the electric drivetrain offers new potentials for vehicle dynamics and chassis control as well. Highly relevant is the capability to recover kinetic energy during braking (*recuperation*), if the electric machine switches to generator mode. Then, the magnetic force points opposite to the motion direction, which slows down the vehicle and the constantly turning rotor produces an electric current, that can be used for recharging the traction battery. Through effective use of this technique, it is already possible to cover most of everyday braking events with decelerations of less than 0.3g. The installed friction brakes are only needed for braking to standstill and for holding the vehicle. To efficiently allocate the brake torque, the so-called (brake) torque blending is used. For implementation of this strategy, several approaches are already known [20, 21, 22, 23, 24, 25, 26, 27, 28, 29]. One of the most challenging tasks is the efficient and safe split of regenerative and friction brake torque, because this depends strongly on brake system architecture and drivetrain properties. Hence it is not simply possible to use one strategy for all kinds of drivetrain layouts and topologies. For instance, the results in [20] relate to a fully electric small passenger car with central electric front drive, while [21] relates to a HEV with power split. Both have unequal potential for energy recovery, so the blending strategy differs. Moreover, the number of driven axles is relevant. The best potential for integrated control is obviously gained by four-wheel drive (4WD) [7, 10, 13, 14, 21, 25, 27, 29] especially with one electric machine per corner [13, 25, 27, 29], since it offers more degrees of freedom. Nevertheless, most vehicles – excepting off-road vehicles and SUVs – do not have this kind of drivetrain topology. Rather, vehicles with two-wheel drive (2WD) are more likely. Due to that, the following article concentrates on a battery electric SUV with 2WD based on in-wheel propulsion.

Besides the choice of suitable vehicle layout, most of the presented studies were carried out in simulation solely, where the integrated controller was modelled in Simulink® [8, 9, 10, 11, 12, 13, 14, 15, 16, 17, 18, 20, 21, 22, 24, 25, 26, 27, 28, 29] and the vehicle dynamics, scenarios as well as environmental conditions were completely virtual and simulated with tools like CarSim [8, 9, 10, 12, 14, 15], Simcenter Amesim [20, 21, 22, 25], CarMaker [13, 24, 25, 29] or Dymola [26]. Of course, the virtual development techniques are beneficial in case of repeatability, safety and robustness and sometimes the only way for testing in case there is no demonstrator available, but it also comes with limitations, since several aspects and especially for e. g., non-linear phenomena (brake pad-disc friction), high-fidelity models are not available or only with a plenty of necessary simplifications and linearization. To consider more complex phenomena, the use of hardware- or test-bench-in-the-loop techniques [25, 28, 30] is advised before tests on vehicle level. Nevertheless, vehicle tests are necessary in the development process to finally prove, if the performance matches the requirements.

Hence, this paper introduces vehicle tests of a battery electric SUV with in-wheel propulsion and hybrid brake-by-wire system under realistic conditions on a driving cycle, see [1]. The structure of the article is given as follows. In the next section, the vehicle prototype and its chassis systems are introduced. Section III describes the control architecture. Section IV outlines driving cycle and the overall methodology. Section V discusses the data and the results from the measurements. Section VI finally summarizes the research and gives an outlook on future potentials.

Vehicle Prototype

The vehicle prototype (see Fig. 1) is based on a 2018 AUDI e-tron, which was equipped with new mechatronic chassis actuators in the framework of the EVC1000 project (https://evc1000.eu). Special interest lies on the new drivetrain: the baseline vehicle features an electric all-wheel drive (AWD) based on two central asynchronous machines, while the demonstrator vehicle in the present study uses rear-wheel drive (RWD) with two high-torque in-wheel machines, based on permanent magnet synchronous machines, powered by a dual inverter with silicon carbide (SiC)-based power stages. This is advantageous with regard to time synchronism, overall packaging, hardware sharing and functional integration. Besides the new drivetrain, the vehicle was equipped with a hybrid, decoupled brake system. It combines electrohydraulic actuators with the original brake calipers on the front axle and electromechanical brake calipers on the rear axle. This axle split is advantageous for several reasons, since the higher dynamics and better controllability of the rear calipers ensure better joint operation between friction brakes and regenerative braking system, which is mandatory for e. g. (brake) torque blending as an essential part of the study. An access to the original vehicle sensors and electronic control units is granted through a new harness, that is connected with the new chassis actuators on the one side and with a SCALEXIO AutoBox from dSPACE on the

FIGURE 1 Vehicle Demonstrator including chassis actuators

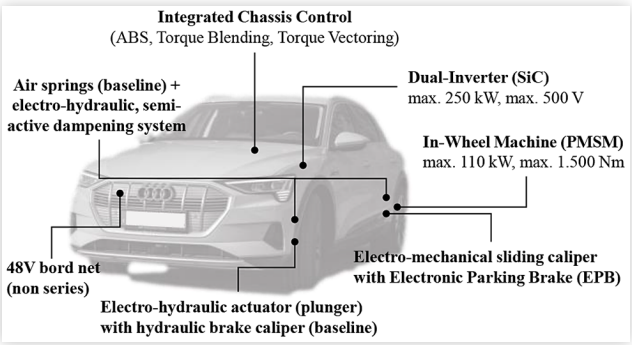

TABLE 1 Technical data of the demonstrator compared to baseline vehicle [1]

Parameter	Unit	baseline	demonstrator
Vehicle total mass	[kg]	2565	2513
Wheelbase	[mm]	2968	
Maximum vehicle speed	[km/h]	200	165
Drivetrain topology	-	AWD	RWD
Electric machine type	-	ASM	PMSM
Machine torque (front axle)			
• nominal value	[Nm]	2200	-
• peak value	[Nm]	2750	-
Machine torque (rear axle)			
• nominal value	[Nm]	2800	1300
• peak value	[Nm]	3120	3000
Overall system power			
• nominal value	[kW]	165	130
• peak value	[kW]	300	220
Tire size	-	255/50 R20 109Y	
Dynamic tire radius	[mm]	371	

other side. This real-time capable processing and data management platform serves as new actuator control unit and stores the integrated high-level chassis controller. The controller and its architecture are described next.

Control Design and Architecture

With removal of the series chassis actuators, it was mandatory to set up the control functions for new components. The control structure equals that one outlined in [1] and was realized in Simulink®. With the Rapid Control Prototyping (RCP) interface *ConfigurationDesk* by dSPACE, Simulink® models can be easily transferred into machine code and downloaded to the processing unit of the SCALEXIO AutoBox. But first, the most relevant functions of the integrated control are discussed. Since this study focusses on (brake) torque blending and its influence on vehicle power consumption, only the braking case is further described.

In a first step, the brake pedal position (BPP) is forwarded to the *Reference Generator*, where the base brake torque (T_{bb}) is calculated out of total brake force (F_{br}), further expressed by vehicle mass (m_v), reference deceleration (a_{ref}), and dynamic tire radius (r_{dyn}). The value of reference deceleration is given by a look-up table in the controller. The shape of the "deceleration-pedal travel" curve is very important, since only a well-modulated brake pedal feeling will be accepted by any driver.

$$T_{bb} = F_{br} r_{dyn} = m_v a_{ref}\left(BPP\right) r_{dyn} \tag{1}$$

The challenge for optimized blending and energy recuperation is an effective brake force distribution (BFD). Due to the dynamic load shift during braking, the dynamic wheel loads on the front axle ($F_{z,f}'$, see Fig. 2) increase and the tires are capable to transmit more braking force to the ground.

The ratio of braking forces on the front ($F_{br,f}$) and rear axle ($F_{br,r}$) and the total amount of dynamic wheel loads

FIGURE 2 Dimensions and forces of the vehicle

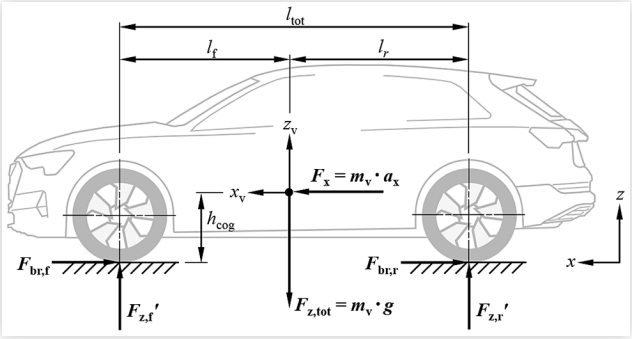

($F_{z,tot}$) is expressed through the braking intensity *z*. Since the braking forces and wheel loads can be expressed by vehicle mass and the values for longitudinal (a_x) and gravitational acceleration (*g*) too, their ratio equals *z* (see eq. (2)).

$$z = \frac{F_{br,tot}}{F_{z,tot}} = \frac{F_{br,f}}{F_{z,tot}} + \frac{F_{br,r}}{F_{z,tot}} = \frac{a_x}{g} \tag{2}$$

The ideal brake force distribution is then expressed by eq. (3). The curve is also depicted in Fig. 3 as red line.

$$\frac{F_{br,r}}{F_{z,tot}} = \sqrt{\left(\frac{l_r}{2h_{cog}}\right)^2 + \frac{l_{tot}}{h_{cog}}\frac{F_{br,f}}{F_{z,tot}}} - \frac{l_r}{2h_{cog}} - \frac{F_{br,f}}{F_{z,tot}} \tag{3}$$

Every BFD on that curve guarantees the optimal use of the friction potential between tire and underground and therefore best braking performance. The green and black lines represent limitations from [31]. For all data points between these lines and the red one, the front wheels lock before the rear ones. Since the rear axle holds the vehicle on track, this situation applies as "stable". The black dashed lines represent constant brake intensity values, so a vehicle's deceleration is constant as long as it remains on a corresponding line. In the cross points with the curve of the ideal BFD, the values equal the road friction coefficient ($z_{id} = \mu$). However, this distribution is not very effective for electrically driven vehicles in terms of regenerative braking, especially for those without 4WD. In [32], the authors show a method for maximized energy recovery for electric vehicles with single front or rear wheel drive and proofed safe braking performance at different brake intensities already. Since the present ICC do not have a road friction estimator, the methodology was slightly adapted, since it uses the demanded brake intensity (a_{ref}/g) and supports fully regenerative braking up to a threshold of $z_{dem} = 0.3$. This threshold was chosen, due to the following reasons:

a. the friction potential between tire and underground is likely higher than $\mu = z_{id} = 0.3$,
b. the maximum torque of the in-wheel machines does not allow higher braking intensities, and
c. the torque blending controller gets deactivated above this mark.

Moreover, it shall be noticed, that safety and stability functions are prioritized in the control architecture, so in

case of unstable vehicle motion, the friction brake system is used solely.

Since the blue line in Fig. 3 cannot be implemented in the controller model due to its infinite slope, an alternative is mandatory. Therefore, the rear brake force is implemented as a function of the demanded brake intensity (see eq. (4)), where x_1 and x_2 are tuning parameters for the gradient of pure rear brake amount and the distance between ideal and installed BFD. In the study x_1 = {0.95, 1.0} and x_2 = 0.006 were investigated. The parameters a and b are the boundaries of the reduction area. In the experiments, the values were set to a = 0.29 and b = 0.31, respectively. This distribution is depicted as blue line in Fig. 3.

$$\frac{F_{br,r}}{F_{z,tot}}\left(z_{dem}\right)=\begin{cases} x_1 z_{dem} & z_{dem}\le a \\ -\frac{h_{cog}}{l_{tot}}z_{dem}^{\,2}+\frac{l_v}{l_{tot}}z_{dem}-x_2 & z_{dem}\ge b \\ \frac{-\frac{h_{cog}}{l_{tot}}b^2+\frac{l_v}{l_{tot}}-bx_2-x_1 a}{b-a}z_{dem}+x_1 a-ma & \text{else} \end{cases} \tag{4}$$

Once, the corner brake torques are generated, the *Integration Logic* adds a reactive torque coming from the *Wheel Slip Controller*, which shall prevent the wheels from blocking. A detailed overview on the controller and its performance in virtual and test bench tests is given in [24, 33, 34] and not further discussed now. The torque demands are then forwarded to the *Torque Distribution Controller*, which is mainly acting as *Torque Blending Controller*, but is also features the function, if the driver accidently hits both pedals at the same time. In that case, a fixed (friction) brake torque is applied to all corners. In case of torque blending, the controller splits the torque demand into separate demands for the electric machines ($T_{em,dem}$) and the friction brakes ($T_{fb,dem}$).

$$\begin{bmatrix} T_{em,dem} \\ T_{fb,dem} \end{bmatrix}=\begin{bmatrix} \mathrm{sat}_0^{\max(T_{em})}\left(\alpha T_{br}\right) \\ T_{br}-T_{em,dem} \end{bmatrix} \tag{5}$$

The variable α is named *blending factor* and used for the allocation of the total brake torque demand between electric machines and friction brakes. In particular, it consists of an initial value ($0 \le \alpha_{init} \le 1$), that firstly decides about the used blending strategy [25] and gets updated then by constraints of the electric machines (e. g., rotational speed, temperature) and the traction battery (e. g., max. charging current, state-of-charge (SOC)) as well as vehicle dynamics (e. g., velocity, requested brake intensity etc.). The output is low-pass filtered, so the blending factor cannot perform steps. Finally, the torque demands are transmitted to the brake control units and the dual-inverter, where low-level controllers generate corresponding signals for the actuators. Sensors in the actuators do measure the actual torques and transmit them to the ICC over CAN to allow a closed-loop control.

Experimental Studies

The tests were carried out on a driving cycle developed by University of Technology Ilmenau for measurement of real driving emissions that was already outlined in [1], but due to temporary construction sites and road closures, it was necessary to slightly adapt the cycle, see Fig. 4. In [1] the total kinetic energy was $2.193 \cdot 10^6$ kJ and now it is $2.296 \cdot 10^6$ kJ (+4.7%), so both data sets can still be compared in an objective benchmark to show the further improvements. Boundaries from [1] are still valid. In total, nine cycles and a regression analysis have been performed to evaluate repeatability and compatibility. All possible combinations showed a regression coefficient of $R^2 > 90\%$.

As already mentioned in previous section, the brake force distribution was optimized with regard to the rear braking amount. Hence, the vehicle is now capable to use regenerative braking more frequently than in [1] during one driving cycle. For x_1 = 0.95 (Fig. 5, (a)) the front axle gets slightly activated in every brake event, resulting in a high number of blended actions, which is ineffective with

FIGURE 3 Ideal (red) and installed brake force distribution (blue)

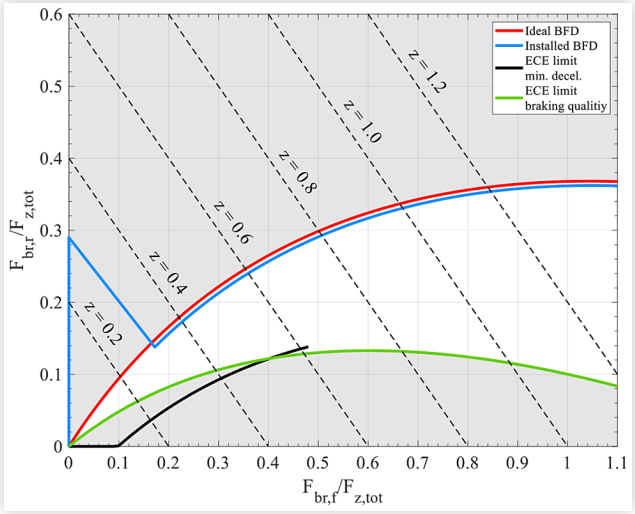

FIGURE 4 RDE driving cycle used in the investigations

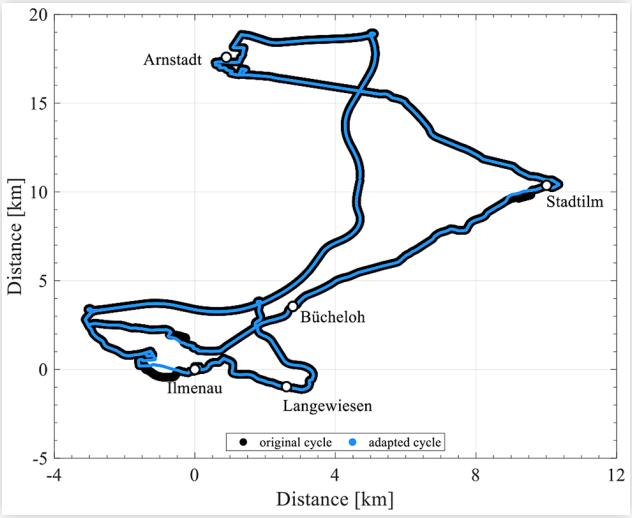

regard to energy recovery and also results in increased brake wear emissions, too.

This setup was used for cycles one to three. The second setup (cycle four to nine) with $x_1 = 1.0$ results in a better performance, represented by three more or less sharply divided sections, showing that nearly all braking events with $z_{dem} < 0.3g$ were covered fully regenerative. Moreover, the hard limit for pure friction braking is located at 10 km/h, which is the configured threshold, so in summary, the control works as expected.

Nevertheless, the amount of blending is still quite high and there is a region, were the vehicle uses both regenerative and blended braking. In the data, this phenomenon can be found between 15 and 55 km/h, so it seems to be related to city driving, see Fig. 6 too. The reason lies in internal control limitations, that are shown in Fig. 7: The blending factor is only updated, when the controller gets active during brake maneuvers, indicated by the brake pedal switch going to "1". Further, the actual blending factor decreases as the vehicle speed falls below a threshold of 20 km/h. This shall ensure a smooth transition between pure regenerative and friction brake torque before the blending is deactivated at vehicle speeds lower than 10 km/h. Finally, the output is low-pass filtered to consider actuator limitations. This leads to a less dynamic response of the blending factor signal after activation of the blending control, see Fig. 7. Especially during city driving, this effect is critical, since the brake is actuated more frequently even at low speeds, so the blending control gets activated quite often, but only for a short duration, which leads to a slowly increasing blending factor signal and more use of the friction brakes in blended mode.

However, to evaluate the effectiveness, the actuators' *braking energy* amounts ($E_{br,act}$) are investigated. Therefore, the kinetic energy during braking events ($E_{kin,br}$) gets multiplied with the ratio of the actuators' torque contributions (T_{act}) and the total brake torque ($T_{br,tot}$).

$$E_{br,act}\left[\text{kJ}\right] = E_{kin,br}\frac{T_{act}}{T_{br,tot}} = \frac{m_v v_v^{\,2}}{2000}\frac{T_{act}}{T_{fb}+T_{em}} \tag{6}$$

FIGURE 5 Brake blending actuation during cycles (a) two and (b) four

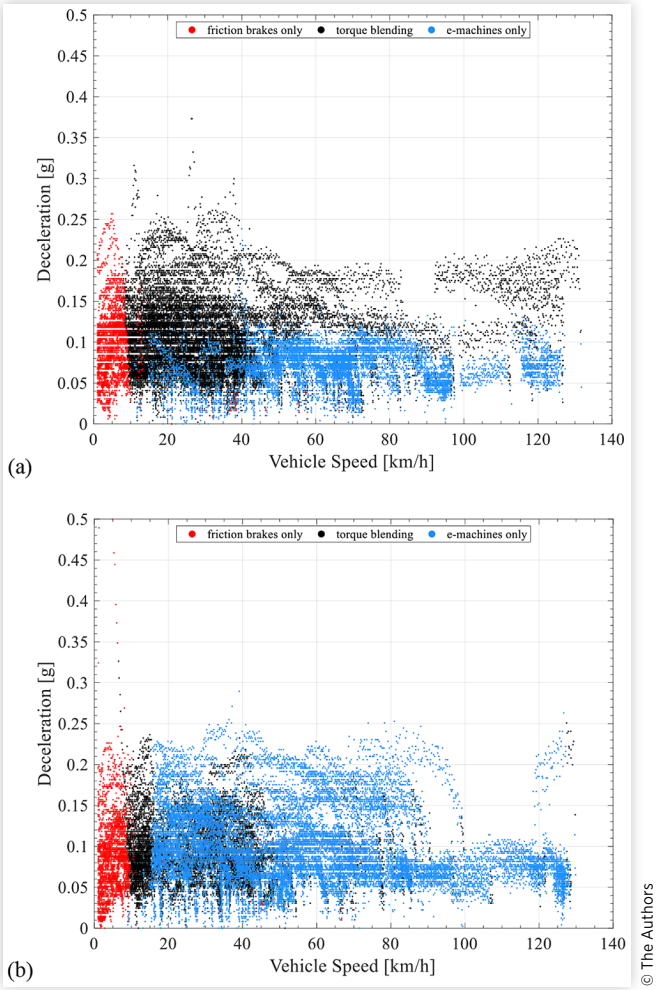

FIGURE 6 Driving cycle with speed profile overlay

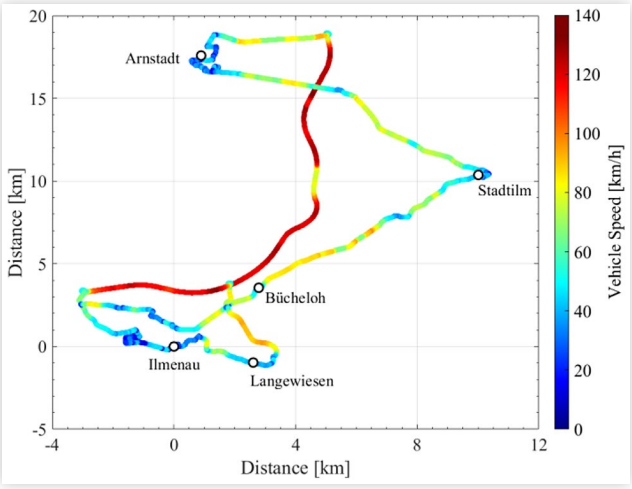

FIGURE 7 Brake blending actuation during brake manoeuver with filter delay

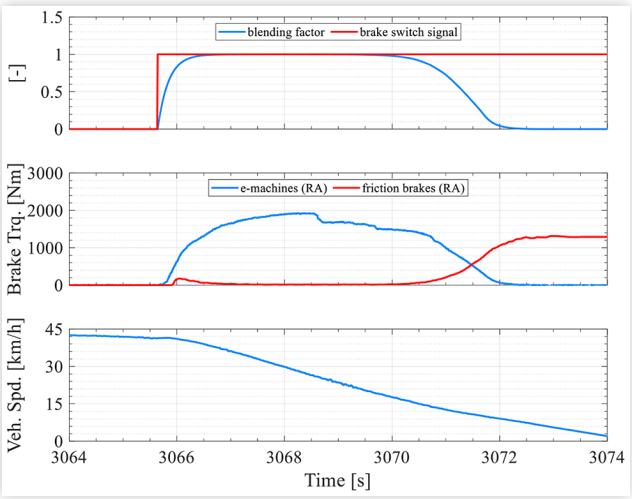

Fig. 8 shows the results with $2.08 \cdot 10^4$ kJ for the electric machines, which is 18.7 times higher than for the friction brakes ($1.05 \cdot 10^3$ kJ). For better comparison against [1], the data are also shown in Fig. 8. Worth noticing, that the new setup increased the regenerative brake energy by an average of 36.8% up to series level with remarkable decrease of the friction brake amount by 24.1%.

To visualize this more practical, a further performance indicator is introduced: The *Regenerative Braking Ratio* (*RBR*) is the ratio of the regenerative braking energy and the kinetic energy, that needs to be dissipated, during the same brake event.

$$RBR\left[\%\right] = \frac{E_{br,em}}{E_{kin,br}} 100 = \frac{200}{m_v {v_v}^2} E_{br,em} \tag{7}$$

In the formerly discussed cycle no. 4, the RBR lies at 95.12%, so less than 5% of all kinetic brake energy during the cycle was dissipated through the friction brakes. Compared to the previous test ride no. 2, an improvement of 2.83% was achieved (see Table 2).

For customers, the brake energy distribution of the brake energy is less interesting, since proper tuning ensures, that the driver does not notice blending. More relevant is the information about the consumed and recovered energy, which is derived from the traction battery's voltage (U_{batt}) and current (I_{batt}) signals.

$$E_{batt}\left[\text{kWh}\right] = \frac{U_{batt}\, I_{batt}}{3.6 \times 10^6} \tag{8}$$

The data is depicted in Fig. 9. Since this value is only valid for this specific driving cycle, it makes sense to use a normalized indicator. Therefore, the ratio of recovered and consumed energy is introduced as *Recovery Index* (*RI*).

$$RI\left[\%\right] = \frac{E_{rec}}{E_{cons}} 100 = \frac{E_{batt}^{+}}{E_{batt}^{-}} 100 \tag{9}$$

Using the above mentioned data, the maximum RI lies at 17.93%, while the controller from [1] results a RI of 12.92%, so another 5% of improvement were achieved.

Even if this information is quite interesting from performance point of view, the more relevant and at least directly noticeable effect is the change of electric energy consumption, which is introduced next. Therefore, the data of the electric energy is normalized by the total driven distance (s_{tot}) and then extrapolated to 100 km. Within the study, the results in Table 3 were achieved.

$$E_{100}\left[\text{kWh / 100km}\right] = \frac{E_{batt}}{s_{tot}} 100 \tag{10}$$

Through the control, the energy consumption on the cycle is nearly equal to the baseline vehicle [1] and is moreover located at the lower border of officially released energy consumption data from [35]. This is quite remarkable, since the baseline vehicle can recover energy at a higher power level due to its electric 4WD, so the optimized brake force distribution and the blending control proofed effectiveness. However, there is no direct comparison made with the baseline vehicle, since without access to the battery CAN, the total energy consumption cannot be calculated following eq. (8). Contrary to [1], the

FIGURE 8 Comparison of the cumulated braking energy for different set-ups

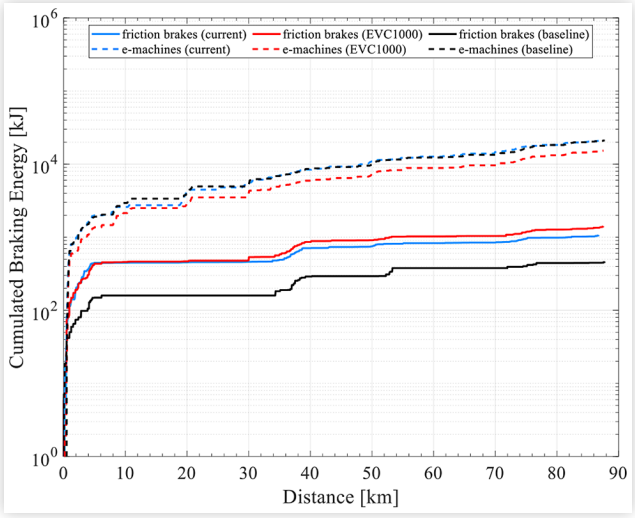

TABLE 2 Results of the cumulated kinetic energy, cumulated braking energy and RBR in comparison

No.	$E_{kin,br}$ [kJ]	$E_{br,em}$ [kJ]	$E_{br,fb}$ [kJ]	*RBR* [%]
1	$1.84 \cdot 10^4$	$1.69 \cdot 10^4$	$1.47 \cdot 10^3$	91.99
2	$2.17 \cdot 10^4$	$2.00 \cdot 10^4$	$1.62 \cdot 10^3$	92.50
3	$1.94 \cdot 10^4$	$1.78 \cdot 10^4$	$1.55 \cdot 10^3$	92.01
4	$2.19 \cdot 10^4$	$2.08 \cdot 10^4$	$1.07 \cdot 10^3$	95.12
5	$1.92 \cdot 10^4$	$1.82 \cdot 10^4$	$1.01 \cdot 10^3$	94.74
6	$2.11 \cdot 10^4$	$1.99 \cdot 10^4$	$1.14 \cdot 10^3$	94.60
EVC1000 [1]	$1.66 \cdot 10^4$	$1.52 \cdot 10^4$	$1.41 \cdot 10^3$	91.56
baseline [1]	$2.15 \cdot 10^4$	$2.11 \cdot 10^4$	$0.46 \cdot 10^3$	98.14

FIGURE 9 Electrical energy amount for cycle no. 4 and the data from [1]

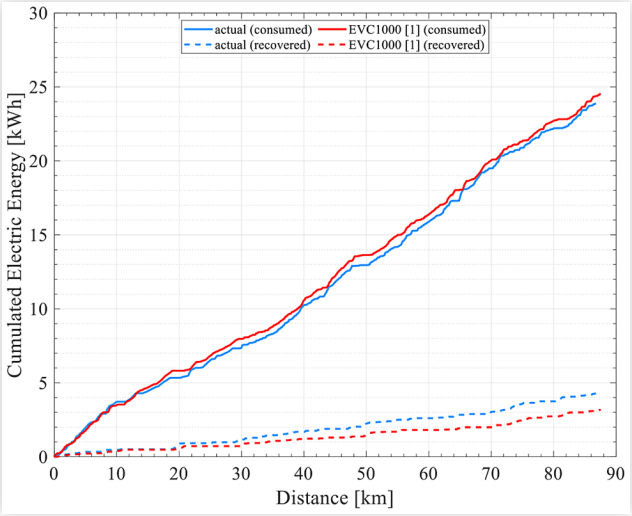

state of charge is not used alternatively, since without precise knowledge about the used reference capacity value of the traction battery, calculation errors and misinterpretation are too likely.

Besides the achieved improvements, the data from Table 3 show how relevant the torque blending is for the overall energy consumption in any case: Ignoring the amounts of recovered energy and extrapolating the consumed energy solely, the total energy consumption grows by a mean of over 12.7%. Other experiments, that were performed by the authors showed also growth by more than 20%.

Drivetrain efficiency investigations After investigating the performance of the integrated braking control, also other aspects shall be considered, that may influence the results. One really critical point is the drivetrain efficiency, so the ratio of mechanical power at the wheel and the electrical power from the energy storage. The current drivetrain contains three components (traction battery, inverter, in-wheel machine), which have a main impact on efficiency, so it makes sense to have a dedicated look to all of them to identify possible impact potentials. Therefore, electrical power (traction battery, inverter) and mechanical power (electric machine) is calculated for these components, see eq. (11) to (13). The electrical power of the electric machine is neglected and it is assumed that is more or less equal to the electrical power of the inverter due to the short cable length. Moreover, the function of the electric machine is the transformation of electrical in mechanical energy and vice versa, so it is sufficient for these experiments to concentrate on this.

$$P_{batt}\left[\text{kW}\right] = \frac{U_{batt} I_{batt}}{1000} \tag{11}$$

$$P_{inv}\left[\text{kW}\right] = \frac{U_{inv} I_{inv}}{1000} \tag{12}$$

$$P_{mech}\left[\text{kW}\right] = \frac{T_{em}\,\omega_{em}}{1000} \tag{13}$$

Fig. 10 depicts the data for one chosen cycle. It can be seen that the efficiency of all components seems to be almost constant during the different sections of the driving cycle. Moreover, it can be noticed that the inverter has a higher efficiency than the in-wheel machine. To

TABLE 3 Results of the recovered and consumed electric energy, recovery index and energy consumption in comparison

No.	E_{rec} [kWh]	E_{con} [kWh]	RI [%]	E_{100} [kWh/100km]
1	3.33	24.07	13.82	23.88
2	4.17	24.47	17.04	23.36
3	3.70	23.88	15.49	23.24
4	4.28	23.88	17.93	22.59
5	3.63	23.23	15.62	22.58
6	3.96	23.79	16.64	22.86
EVC1000 [1]	3.17	24.53	12.92	24.40

FIGURE 10 Power level data of the drivetrain components during one cycle

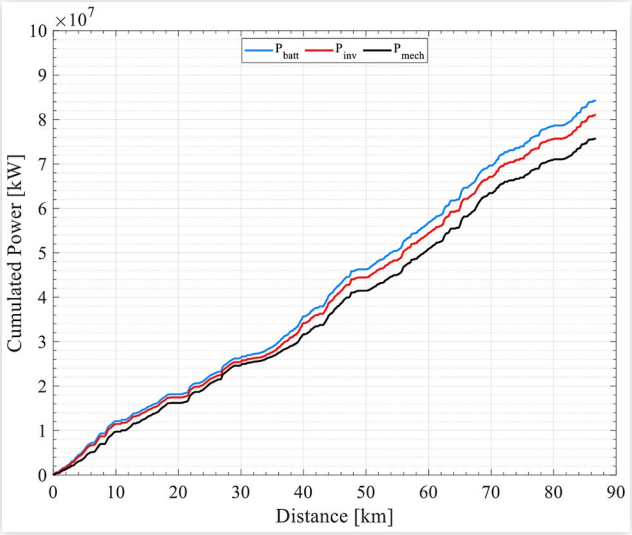

quantify that, the *Component Efficiency Ratio* (η) is introduced as performance indicator given by the power in- (P_{in}) and output (P_{out}).

$$\eta\left[\%\right] = \frac{P_{out}}{P_{in}} 100 \tag{14}$$

For the inverter the ratio P_{inv}/P_{batt} equals approx. 96%, while the in-wheel machines (P_{mech}/P_{inv}) finally come to approx. 92%. Generally, the values are matching those in [36] and resulting in an overall system efficiency ratio of ca. 88.3%. In that special case, the battery efficiency (based on cell chemistry and layout) was not considered due to missing information, but taking into account a usual efficiency ratio of max. 96% [36], the overall ratio lies at 84.8%. Moreover, deviations due to wheel slip are neglected in this study, but it is expected, that the results are not significantly affected.

Influence of thrust recuperation In the previously shown studies, the vehicles uses "sailing mode" all the time, so when releasing the pedals, the electric machines switch into idle mode and the only effect that slows down the vehicle is the driving resistance. In this mode, the vehicle does not consume any energy from the traction battery, but also regeneration is not used. Since more and more electric vehicles already feature "one-pedal driving", this function was implemented to the present ICC too. In this mode, which shall be called *thrust recuperation* in the framework of this article, a regenerative torque is requested from the electric machines when the drive pedal is released. This torque activates the energy recovery. The higher the requested amount, the higher is the recovery potential, but also the deceleration of the vehicle. If connected to other assistance, sensing or navigation systems, the amount can be applied adaptively for optimal performance. In the current case, two different amounts were investigated: a) 550 Nm (low) and b) 1050

FIGURE 11 Comparison of the electrical energy amount for different set-ups

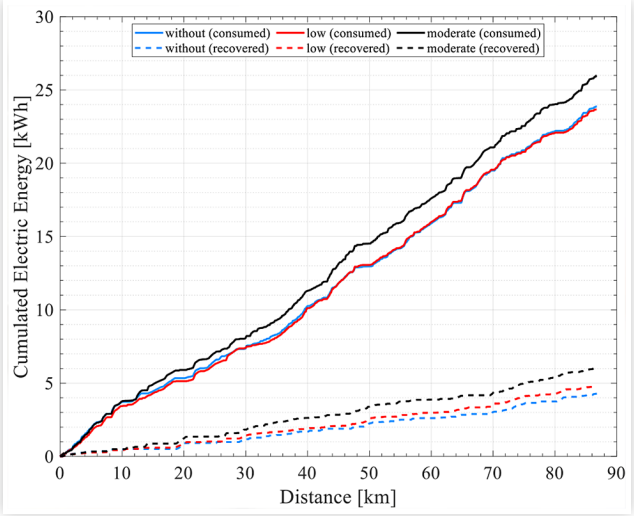

Nm (moderate). The values are derived from [37], where it is said that it equals those from the baseline vehicle. Fig. 11 shows the graphs for the consumed and recovered electric energy divided by the different thrust recuperation modes. Table 4 contains the corresponding numerical values.

From the data, it is worth noticing that with the thrust recuperation (low) the *Recovery Index* increased by ca. 3%, while the consumed energy stays nearly the same as before. This results in an energy saving of ca. 0.94 kWh/100km (-4.15%). Much more interesting is the case with the higher torque request: Even that the *Recovery Index* is 3% higher than before and the recovered energy amount increases by 26.25%, the overall energy consumption also increases. This is due to the necessity of reaccelerating the vehicle more frequently to stay within the boundaries of RDE conformity in this case. Due to the lower deceleration effect with the low thrust recuperation, the vehicle speed boundaries are not violated that often. Moreover, the stronger thrust recuperation was percept as more uncomfortable during the ride, so the ride was not repeated after the first run. For future studies, there should be any kind of logic, which varies the requested torque amount adaptively with regard to vehicle state and vehicle dynamics.

TABLE 4 Results of the recovered and consumed electric energy, recovery index and energy consumption in comparison

No.	E_{rec} [kWh]	E_{con} [kWh]	*RI* [%]	E_{100} [kWh/100km]
7	4.80	23.68	20.27	21.77
8	4.74	23.56	20.14	21.70
9	6.06	25.98	23.33	22.96

Summary / Conclusions

This article presented real-world test of an integrated chassis control with optimized brake force distribution, tailored for rear-wheel driven, battery electric vehicles, as well as (brake) torque blending functionality. The control was implemented in Simulink®, compiled to machine code via RCP interface and then flashed on a SCALEXIO AutoBox installed in a vehicle demonstrator equipped with hybrid brake-by-wire system and innovative, in-wheel propulsion based drivetrain. With this demonstrator, vehicle tests were carried out on public road on a RDE conform driving cycle developed by University of Ilmenau to evaluate and quantify the controller's performance.

Through the optimized brake force distribution, it was possible to reduce the use of the friction brake system and to decompose more than 95% of kinetic brake energy with the electric machines. This surely leads to an energy recovery potential improvement of 8.9% compared to [1] and the overall power consumption was lowered by over 4% against the experiments without thrust recuperation.

Moreover, the potential of thrust recuperation was investigated as possible enhancement of the control. Therefore, two different modes were implemented and tested. The first one with a torque demand of 550 Nm showed good results: the energy recovery was increased by 3%, giving and overall improvement of nearly 12%. The second mode was percept as uncomfortable and resulted in a higher energy consumption, since the vehicle speed was about to violate boundaries given by the RDE guidelines. Therefore, the vehicle was accelerated more frequently, resulting in a "worse" energy efficiency. Since the baseline vehicle from [1, 37] uses the same torque demand by using thrust recuperation, possible use cases need to exist. Further it would be interesting to investigate and compare the vehicle dynamics of both vehicles to see if it is possible to simply replicate the torque demands without consideration of the different drivetrain layouts of the vehicles. If not, suitable amounts need to be found for the demonstrator vehicle. Further experiments on this topic are currently under preparation by the authors and carried out for future research.

Since the research mainly aims to improve vehicle efficiency, it is beneficial to create comparability between demonstrator and baseline vehicle regarding the energy consumption measurement to show the improvements made by the new chassis actuators and integrated control. Currently, the baseline vehicle features the measurement of battery SOC solely, which gives a less dynamic feedback. Table 5 shows the difference between the calculation based on SOC (see [1]) and based on eq. (8) and eq. (10). It can be seen, that the deviations alternate, so no clear trend can be identified. Moreover, the peak-to-peak error is nearly 11%, covering the potential shown in this study, so the SOC method shall be replaced consequently, since without deeper knowledge, it is nearly impossible to calculate the correct values.

TABLE 5 Results of the recovered and consumed electric energy, recovery index and power consumption in comparison

No.	s_{tot} [km]	E_{100} (SOC) [kWh/100km]	E_{100} (eq. (8)) [kWh/100km]	ΔE_{100} [%]
1	86.90	22.72	23.88	-4.88
2	86.88	23.62	23.36	1.11
3	86.85	24.06	23.26	3.44
4	86.77	20.86	22.59	5.94
5	86.79	19.60	22.58	-4.97
6	86.74	20.06	22.86	0.90
7	86.74	19.03	21.77	-4.23
8	86.72	20.00	21.70	1.13
9	86.76	20.81	22.96	-0.68
EVC1000 [1]	87.54	22.68	24.40	-7.05

Regarding the results already achieved, the remaining potential for further improvement and increased energy recovery through braking solely becomes lower. Therefore, some experiments for the drivetrain efficiency were performed. It was shown that it lies above 88% already and that the lowest component efficiency comes from the in-wheel machines. Due to the fact that the obtained values match the results from the previous studies in [36] as well as the data from the component suppliers, other methods need to be found.

One possibility is to make the controller more adaptive to vehicle state and environmental influences. In the experiments with moderate thrust recuperation, the overall performance was worse than before. Nevertheless, this mode may be beneficial during driving in the city, where one-pedal driving with higher deceleration is accepted due to stop-and-go traffic. Hence, some everyday use cases can be covered without brake pedal e. g., rolling towards a red traffic light. So an *adaptive recuperation mode*, where the controller switches between different torque demands, depending from the vehicle speed and state are interesting. Corresponding tests shall be covered within the mentioned experiments on thrust recuperation in future.

For statistic reliability, the course needs to be driven more times. Due to varying traffic on the track, it is beneficial to do measurements at different times (morning, noon, evening, night). Additionally, the influence of different drivers would be interesting to investigate as well as a direct comparison with the benchmark vehicle driving on the same track at the same time as performed in [1].

References

1. Heydrich, M., "Investigations on the Energy Saving Potential of X-by-Wire Chassis Systems and Advanced Integrated Control Strategies," in *6th Electric Vehicle Technology Conference (EVTeC), Conference Paper*, 2023.
2. Mazzilli, V., De Pinto, S., Pascali, L., Contrino, M. et al., "Integrated Chassis Control: Classification, Analysis and Future Trends," *Annual Reviews in Control* 51 (2021): 172-205.
3. Bertram T., *Vernetzung von Längs-, Quer- und Vertikaldynamik-Regelung*, In: Fahrdynamikregelung. Modellbildung, Fahrerassistenzsysteme, Mechatronik, vol. 1, Rolf Isermann, 2006.
4. Yu, F., Li, D.-F., and Crolla, D.A., "Integrated Vehicle Dynamics Control – State-of-the-Art Review," in *IEEE Vehicle Power and Propulsion Conference (VPPC), Conference Paper*, 2008.
5. Vivas-López, C.A., Hernández-Alcantara, D., Tudón-Martínez, J.C., and Morales-Menendez, R., "Review on Global Chassis Control," in *5th IFAC Symposium on System Structure and Control*, 2013.
6. van Zanten, A.T., "Evolution of Electronic Control Systems for Improving the Vehicle Dynamic Behavior," 2002.
7. Heo, H., Joa, E., Yi, K., and Kim, K., "Integrated Chassis Control for Enhancement of High Speed Cornering Performance," *SAE International Journal of Commercial Vehicles* 8, no. 1 (2015): 102-109.
8. Nah, J. and Seongjin, Y., "Optimization of Control Allocation with ESC, AFS, ARS and TVD in Integrated Chassis Control," *Journal of Mechanical Science and Technology* 33, no. 6 (2019): 2941-2149.
9. Hwang, T., Park, K., Heo, S.-J., and Lee, S., "Integrated Chassis Controller Design of Active Steering and Active Braking Systems Using CL Method," in *International Conference on Intelligent Computing, Conference Paper*, 2007.
10. Her, H., Joa, E., Yi, K., and Kim, K., "Integrated Chassis Control for Optimized Tyre Force Coordination to Enhance the Limit Handling Performance," *Proceedings of the Institution of Mechanical Engineers, Part D: Journal of Automobile Engineering* 230, no. 8 (2015).
11. Elmarakbi, A., Rengaraj, C., Wheately, A., and Elkady, M., "New Integrated Chassis Control Systems for Vehicle Handling Performance Enhancement," *International Journal of Dynamics Control* 1 (2013): 360-384.
12. Yim, S., "Integrated Chassis Control with Four-Wheel Independent Steering under Constraint on Front Slip Angles," *IEEE Access* 9 (2021): 10338-10347.
13. Ahn, T., Lee, Y., and Park, K., "Design of Integrated Autonomous Driving Control System that Incorporates Chassis Controllers for Improving Path Tracking Performance and Vehicle Stability," *Electronics* 10, no. 2 (2021): 144-165.
14. Yim, S., and Yi, K., "Design of Active Roll Control System and Integrated Chassis Control for Hybrid 4WD Vehicles," in *14th International IEEE Conference on Intelligent Transportation Systems (ITSC), Conference Paper*, 2011.
15. Kolte, S., Srinivasan, A., and Srikrishna, A., "Development of Decentralized Integrated Chassis Control for Vehicle Stability in Limit Handling," *In: SAE International Journal on Vehicle Dynamics, Stability, and NVH* 1, no. 1 (2017): 1-10.
16. Elhefnawy, A., Sharaf, A.M., Ragheb, H., and Hegazy, S., "Design of an Integrated yaw-Roll Moment and Active Front Steering Controller Using Fuzzy Logic Control," *SAE International Journal on Vehicle Dynamics, Stability, and NVH* 1, no. 2 (2017): 270-282.

17. March, C. and Shim, T., "Integrated Control of Suspension and Front Steering to Enhance Vehicle Handling," *Proceedings of the Institution of Mechanical Engineers, Part D: Journal of Automobile Engineering* 221, no. 4 (2006): 377-391.
18. Yim, S. and Jo, Y.H., "Integrated Chassis Control with AFS, ARS and ESC under Lateral Constraint on AFS," *JMST Advances* 1 (2019): 13-21.
19. Wei, J., Zhuoping, Y., and Lijun, Z., "Integrated Chassis Control System for Improving Vehicle Stability," in *IEEE International Conference on Vehicular Electronics and Safety, Conference Paper*, 2006.
20. Berzi, L., Favilli, T., Pierini, M., Pugi, L. et al., "Brake Blending Strategy on Electric Vehicle co-Simulation between MATLAB Simulink and Simcenter Amesim," in *IEEE 5th International forum on Research and Technology for Society and Industry (RTSI), Conference Paper*, 2019.
21. Geng, C., Ning, D., Guo, L., Xue, Q. et al., "Simulation Research on Regenerative Braking Control Strategy of Hybrid Electric Vehicle," *Energies* 14, no. 8 (2022).
22. Xu, W., Chen, H., Zhao, H., and Ren, B., "Torque Optimization Control for Electric Vehicles with Four in-Wheel Motors Equipped with Regenerative Braking System," *Mechatronics* 57 (2019): 95-108.
23. Chu, L., Chang, C., Zhao, D., and Xu, Y., "Research on Cooperative Braking Control Algorithm Based on Nonlinear Model Prediction," *World Electric Vehicles Journal* 12, no. 4 (2021).
24. Heydrich, M., Ricciardi, V., Ivanov, V., Mazzoni, M. et al., "Integrated Braking Control for Electric Vehicles with in-Wheel Propulsion and Fully Decoupled Brake-by-Wire System," *Vehicles* 3, no. 2 (2021): 145-161.
25. Ivanov, V., Beliautsou, V., Schreiber, V., Heydrich, M. et al., "Brake Blending Design Using Distributed and Shared X-in-the-Loop Test Environment," in *IEEE Vehicle Power and Propulsion Conference (VPPC), Conference Paper*, 2022.
26. de Castro, R., Araújo, R.E., Tanelli, M., Savaresi, S.M. et al., "Torque Blending and Wheel Slip Control in EVs with in-Wheel Motors," *International Journal of Vehicle Mechanics and Mobility* 50 (2012): 71 -94.
27. Pugi, L., Favilli, T., Berzi, L., Locorotondo, E. et al., "Application of Regenerative Braking on Electric Vehicles," in *2019 IEEE International Conference on Environment and Electrical Engineering and 2019 IEEE Industrial and Commercial Power Systems Europe (EEEIC / I&CPS Europe), Conference Paper*, 2019.
28. Zhang, J.-Z., Chen, X., and Zhang, P.-J., "Integrated Control of Braking Energy Regeneration and Pneumatic Anti-Lock Braking," *Proceedings of the Institution of Mechanical Engineers, Part D: Journal of Automobile Engineering* 224, no. 5 (2009): 587-610.
29. Ricciardi, D.S., Augsburg, K., and Ivanov, V., "Estimation of Brake Friction Coefficient for Blending Function of Base Braking Control," In: *SAE International Journal on Passenger Cars – Mechanical Systems* 10, no. 3 (2017): 774-785.
30. Lv, C., Zhang, J., Li, Y., and Yuan, Y., "Regenerative Braking Control Algorithm for an Electrified Vehicle Equipped with a by-Wire Brake System," SAE Technical Paper 2014-01-1791 (2014). https://doi.org/10.4271/2014-01-1791.
31. Economic Commission for Europe, "ECE-R13H: Uniform Provision Concerning the Approval of Vehicles of Categories M, N and O with Regard to Braking," 2008.
32. Spichartz, P., Xu, B., and Sourkounis, C., "Optimized Recuperation Strategies for Single Front and Rear Wheel Drives," in *Vehicle Power and Propulsion Conference (VPPC)*, 2017.
33. Heydrich, M., Ivanov, V., Bertagna, A., Rossi, A. et al., "Hardware-in-the-Loop Testing of a Hybrid Brake-by-Wire System for Electric Vehicles," *SAE Int. J. Veh. Dyn., Stab., and NVH* 6, no. 4 (2022): 477-487. https://doi.org/10.4271/10-06-04-0031.
34. Heydrich, M., Ivanov, V., Rossi, A., Bertagna, A. et al., "Experimental Studies on Hybrid Decoupled Brake System Functions for Electric Vehicle with in-Wheel Motors," in *15th International Symposium on Advanced Vehicle Control (AVEC)*, 2022.
35. Gramstat, S. et al. "Report on Vehicle and Component Specifications," project report, 2019. URL: https://cordis.europa.eu/project/id/824250/results (20/10/2023).
36. Tschöke, H., *Die Elektrifizierung Des Antriebsstrangs* (Springer Vieweg, 2014)
37. Herklotz, J., "Grundlegende Untersuchungen zu der rekuperativen Betriebsweise von Radbremsen im realen Fahrversuch," Master thesis, 2022.

Contact Information

Marius Heydrich,
Technische Universität Ilmenau
marius.heydrich@tu-ilmenau.de

Thomas Mitsching,
Technische Universität Ilmenau
thomas.mitsching@tu-ilmenau.de

Matthias Lenz,
Technische Universität Ilmenau
matthias.lenz@tu-ilmenau.de

Valentin Ivanov
Technische Universität Ilmenau
valentin.ivanov@tu-ilmenau.de

Sebastian Gramstat
AUDI AG
sebastian.gramstat@audi.de,

Acknowledgement

The research leading to these results was funded by the European Union under the Horizon 2020 Research and Innovation Programme under Grant Agreement No. 824250 (EVC1000) and the Horizon Europe Research and Innovation Programme under Grant Agreement No. 101056824 (HighScape). Views and opinions expressed are however those of the author(s) only and do not necessarily reflect those of the European Union or the European Climate, Infrastructure and Environment Executive Agency (CINEA). Neither the European Union nor CINEA can be held responsible for them.

e-ISSN 2641-9645